LOCAL ATOMIC AND ELECTRONIC STRUCTURE OF
QUANTUM DOTS BASED ON Mn- AND Co-DOPED ZnS

A. N. Kravtsova, A. P. Budnik, I. A. Pankin,
T. A. Lastovina, A. L. Bugaev, L. D. Popov,
M. A. Soldatov, V. V. Butova, and A. V. Soldatov

Solid solutions of zinc sulfide with manganese and cobalt are synthesized. Based on the analysis of X-ray diffraction profiles the conclusion is drawn about the formation of a hexagonal wurtzite type structure in the synthesized quantum dot (QD) solutions. The average crystallite sizes are 8 nm and 22 nm for the samples with manganese and cobalt respectively. Results of IR and optical spectroscopy are consistent with the powder X-ray diffraction and X-ray fluorescence data. The question about particle aggregation in isopropanol and DMF solutions is considered. The QD structures based on ZnS particles doped with Mn and Co transition metal atoms are modeled. The possibility to apply X-ray absorption near edge structure (XANES) spectroscopy to verify the atomic structure parameters around the positions of doping transition metal atoms in QDs of the ZnS family is shown. Partial densities of ZnS:Mn and ZnS:Co electronic states are calculated.

INTRODUCTION

Quantum dots (QDs) are considered to be nanosized semiconductor crystals, usually consisting of II-VI, III-V, or IV-VI group elements [1]. Many efforts are focused on the determination of the relationship between the size, shape, and electronic properties of QDs [2, 3] to gain the possibility of affecting their optical characteristics. Rapid development of nanotechnologies makes it possible to relatively easily obtain efficient QDs, noticeably being ahead of the elaboration of the corresponding theoretical models. Furthermore, often some research groups perform experimental investigations and the others are concerned with theoretical ones. This work presents the experience of parallel theoretical and experimental studies of ZnS based QDs.

Zinc sulfide is an important material for semiconductor electronics, however, nanostructures based on it remain less studied in comparison, e.g., with zinc oxide [4]. Manganese and isovalent impurity doping chemical methods, ion implantation, or thermal evaporation makes it possible to obtain an efficient light emitting material [5] or a diluted magnetic

semiconductor (DMS) combining unique magnetic and optical properties [6]. These properties are, of course, related to the features of the QD structure with impurity atoms, the theoretical study of which remains a relevant problem.

It should be noted that theoretical methods based on density functional theory (DFT) contain a number of approximations, including those determined by the choice of the exchange-correlation potential, and to verify the structural parameters experimental methods are needed. For nanosized objects the appropriate modern method providing the complete three-dimensional information (bond lengths and angels) around the absorbing atoms is X-ray absorption near-edge structure spectroscopy (XANES) [7]. The method of extracting structural information from XANES spectra is indirect; within the analysis the XANES spectra are calculated and the most probable structural model is selected. Recently, the sensitivity of XANES spectroscopy to small changes in the structural parameters of QDs of CdS and CdTe families was shown [8-10]. It is expected that structural changes in the ZnS lattice due to the introduction of Mn or Co impurity atoms are also reflected in the corresponding XANES spectra.

In the past, a large number of works were devoted to the investigation of colloidal ZnS particles [11], the main attention being paid to the photocatalytic and photochemical aspects for applying QDs in solar energy converters. The industrial use of Mn^{2+}-doped ZnS (ZnS:Mn) in thin film electroluminescent devices has stimulated the research interest in the photophysical properties of this system. In particular, Sooklal et al. [12] considered the optical properties of the ZnS:Mn system where manganese (taken up to 5% with respect to Zn^{2+}) was located on the ZnS particle surface in the first case, and in the second case, inside the particle, substituting for zinc. Karar et al. [13] paid attention to that the formation of ZnO on the surface of the ZnS particle can enhance photoluminescence owing to the reduction in the number of non-radiative recombination centers.

With the extension of the QD application field in electronics and biomedicine, in the increasing number of experimental works the authors try to guarantee the dispersion of samples by particle surface modification due to the use of thiols or surfactants in the synthesis [14]. Cao et al. employed a popular method for obtaining CdS QDs by means of reverse micelles, which is based on the surfactant action, to prepare ZnS:Mn particles coated with ZnS [15]. He confirmed that both ZnS shell and UV light allow the improvement of the ZnS:Mn QD luminescence because of the particle surface passivation.

In this work, ZnMnS and ZnCoS QDs were prepared and the obtained samples were completely characterized. The local atomic structure was optimized for the case of introducing Mn or Co atoms into the ZnS structure, which have an uncompensated magnetic moment. For the structural models of ZnMnS and ZnCoS particles the XANES spectra were calculated based on the full potential finite difference method.

EXPERIMENTAL

The reagents were of analytical grade and were not subjected to the additional purification. ZnMnS and ZnCoS QDs were prepared by the modified procedure [16], using the molar ratio Zn:Mn:S = Zn:Co:S = 1.5:1.0:2.5. To an aqueous solution containing 0.033 mol of sodium sulfide an aqueous solution of manganese acetate (0.013 mol) or cobalt acetate (0.013 mol), containing 0.05 ml of thioglycolic acid was added with stirring. The obtained mixture was stirred for 20 min at a temperature of 80 °C, and then the aqueous zinc acetate solution (0.0198 mol), containing 0.055 ml of thioglycolic acid, was added. The mixture was stirred for 8 h at the same temperature. After this the mixture was filtered, twice washed with distilled water, and dried.

The X-ray fluorescence (XRF) analysis of the samples was carried out on an M4 Tornado Micro-XRF (Bruker) spectrometer; the samples in the form of pressed powders were measured on silicon substrates. Electron microscopic examinations were conducted on a Tecnai G2 Spirit BioTWIN transmission electron microscope (TEM) with an accelerating voltage of 120 kV. Powder X-ray diffraction patterns were measured with a step of 0.02° on an ARL X′TRA system (Thermo Scientific), using CuK_α radiation ($\lambda = 1.540562$ Å) at 40 kV and 30 mA. The particle sizes were measured in solutions by photon-correlation spectroscopy and dynamic light scattering (DLS) on a NanoFLEX (Microtrac) particle size analyzer with a semiconductor laser (wavelength 780 nm, power 3 mW). The scattering was investigated at an angle of 180º with analyzing

the spectral density of the Doppler shift range; the temperature in the cuvette was controlled by a high-precision Peltier element. IR spectra were measured on a FSM-1202 (Infraspek) Fourier spectrometer with a resolution of 2 cm^{-1} and averaged over 32 runs. The samples were mixed with KBr in the 1:300 weight ratio and pressed in 1 mm thick pellets. The absorbance spectra were measured in the diffuse reflection geometry on a UV-2600 (Shimadzu) spectrophotometer with a step of 2 nm.

CALCULATION PROCEDURE

A spherical fragment of the wurtzite phase of crystalline ZnS [17], consisting of 68 atoms, was considered as the initial structure of the ZnS particle. The structure of the ZnS particle was optimized based on DFT with the use of periodical boundary conditions and the pseudopotential approximation. This approach was implemented in VASP5.3 (Vienna Ab-initio Simulation Package) [18]. To construct the structure of ZnS particles with incorporated Mn and Co atoms the optimized model of the ZnS particle, in which the central Zn atom was replaced by a Mn or Co atom respectively, was used. Thus constructed structural models of ZnS:Mn and ZnS:Co particles were also optimized using the VASP5.3 code. All calculations were carried out using the PAW-PBE type pseudopotentials (Projector Augmented-Wave Perdew–Burke–Ernzerhof) [19, 20]. Self-consistent field (SCF) cycles of the electron density were calculated by means of the Dawson function. The energy factor of the convergence of ionic relaxation cycles was $1.5 \cdot 10^{-4}$ eV. The basis set of plane waves was limited to an energy of 400 eV.

The VASP5.3 code was intended to model the atomic and electronic structures of periodic systems within the ground state of the electronic system. It is necessary to take into account the core vacancy caused by the electronic transition for the correct description of X-ray absorption spectra near K-edges of metals [21]. Therefore, to take into account the core vacancy, the XANES spectra near the manganese K-edge and the cobalt K-edge of ZnS:Mn and ZnS:Co particles were calculated based on the full-potential finite difference method implemented in the FDMNES program [22]. We have employed the recently updated version of the FDMNES code [23], which enables a substantial reduction of the computational capacity of calculations of absorption spectra in the full potential, using Sparce Solvers in the diagonalization of the finite difference matrix. XANES spectra were calculated using the model of the exchange-correlation potential of the Hedin–Lundkvist type.

Since the calculations with the FDMNES program code were not self-consistent, the calculations of total and partial densities of states (DOS) near the bottom of the conduction band and the top of the valence band of Mn- and Co-doped ZnS clusters were performed based on the full multiple scattering method in the direct space, which was implemented in the FEFF8.4 program [24]. DOS were calculated in the ground state of the electronic system for the optimized structures of clusters consisting of 68 atoms. For comparison, DOS were also calculated for the wurtzite phase of crystalline ZnS [17].

The simulation of the QD structure and the calculations of XANES spectra were carried out on a Blokhin supercomputer at the International Research Center "Smart materials"; DOS were calculated using the IBMX cluster of the Southern Federal University.

RESULTS AND DISCUSSION

The composition of the synthesized samples was controlled by XRF. For the ZnMnS sample it revealed the weight ratios Zn:Mn:S = 41.7:31.1:27.2 (wt.%), which corresponds to the molar ratio 1.0:1.0:1.5. For ZnCoS the weight and molar ratios were Zn:Co:S = 46.1:34.4:19.2 (with 0.4% Si in residue) and 1.3:1.0:1.6 respectively. Comparing with the molar ratio of components in the case of the reaction completion (1.5:1.0:2.5), it is possible to note a decrease in the zinc and sulfur contents with respect to the doping component in both cases of the final product.

According to the TEM image (Fig. 1*a*), the obtained ZnMnS sample consists of partially aggregated isometric particles. A study of the dispersive composition made it possible to construct the QD size distribution in the range from 9.3 nm to 20.1 nm (Fig. 1*b*). The histogram allows the calculation of the average weighted particle size as 13.2 nm.
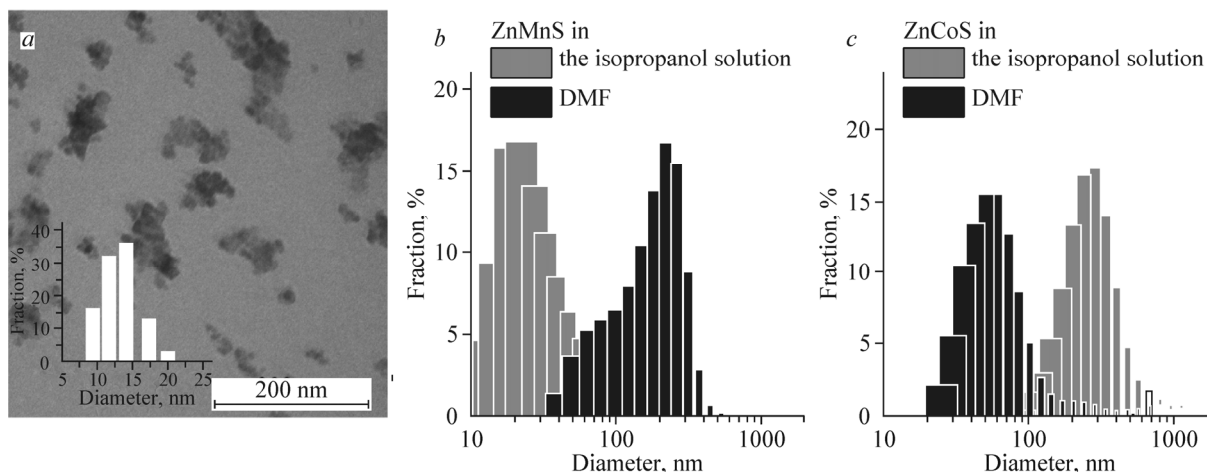
Fig. 1. TEM image of the ZnMnS sample with the particle size distribution (*a*), hydrodynamic particle radius from the DLS data in isopropanol (gray) and DMF (black) solutions for ZnMnS (*b*) and ZnCoS (*c*) samples.

The particle size in the solution was estimated from the DLS data (Fig. 1*c*). For the preparation of colloidal solutions an ultrasound homogenizer was used. For the ZnMnS QD solution in isopropanol the histogram of the particle size distribution demonstrates the maximum number of particles with a hydrodynamic diameter of ~20 nm. With regard to the TEM data, this corresponds to the situation when the majority is composed of single particles and small aggregates. When the aprotic polar solvent is used, such as DMF, a higher degree of aggregation is observed with the maximum position at ~200 nm. For ZnCoS QD an opposite situation is observed: in isopropanol the maximum is located at ~240 nm and in DMF at ~50 nm. This may give evidence of differences in the chemical properties of particle surfaces of the two samples, which results in the observed distinctions in QD solvation.

X-ray diffraction data show (Fig. 2) that the obtained samples contain a hexagonal phase (space group $P6_3mc$) of the wurtzite type (marked by Miller indices in Fig. 2*a*) along with the orthorhombic impurity phase. The hexagonal symmetry is known to be typical of many sulfides, and in particular, for pure MnS, ZnS, and CoS. However, the unit cell parameters of our samples differ from the reference data (Table 1): for ZnMnS obtained the *a* and *c* parameters are larger than those for ZnS, but smaller than those for MnS; the parameters of ZnCoS are lower than those for ZnS. This permits the assumption that the synthesized materials are solid solutions. In this case, the calculated unit cell parameters are consistent with an increase in the ionic radii in the order Co^{2+}, Zn^{2+}, and Mn^{2+} (0.77-0.87 Å) [25]. Moreover, the doubling of reflections at characteristic angles is not observed in diffraction patterns, which would occur for a mechanical mixture of one-phase simple sulfides.
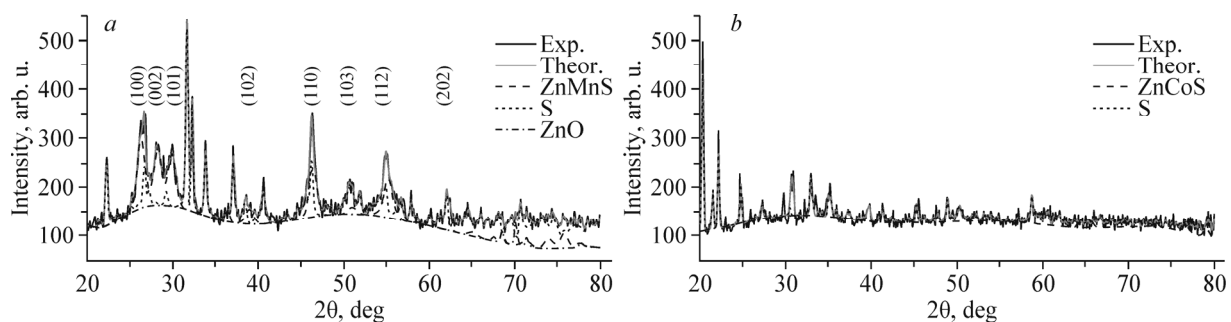

Fig. 2. Experimental diffraction profile of the ZnMnS sample (black solid line), theoretical profile (gray solid line) obtained by the convolution of profiles of the ZnMnS solid solution (dashed line), sulfur (dot-and-dash line), and ZnO (dotted line). Miller indices are given for the phase of the wurtzite type of the ZnMnS sample (*a*); corresponding profiles for the ZnCoS sample (with the same legend) (*b*).

TABLE 1. Unit Cell Parameters of Synthesized ZnMnS and ZnCoS Samples from the Powder X-ray Diffraction Data and Also of ZnS, MnS, CoS Compounds from the Literature Data and the PDF-2 Database

Compound	a, Å	c, Å	Reference	Compound	a, Å	c, Å	Reference
ZnMnS	3.92	6.35	–	ZnS	3.820	6.260	[17]
ZnCoS	3.78	6.29	–	MnS	3.979	6.447	[26]
				CoS	3.377	5.150	[27]

In order to reveal the nature of the impurity phase a full-profile analysis of diffraction patterns was conducted by the Rietveld method using the Jana2006 code. Lattice parameters of probable phases and their relative concentrations, a zero shift correction, 10-parameter Legendre polynomial were used as variables to describe the background and the pseudo Voigt function was applied to describe the profile features. Based on the synthesis features, the occurrence of sulfur- and zinc-containing impurities in the final product, which were not removed by washing, was assumed. As a result of the performed analysis, by the convolution of the profiles of the ZnMnS solid solution, sulfur, and zinc oxide a theoretical diffraction pattern was obtained (Fig. 2a) whose profile coincides well with the experimental one. The average crystallite size was 8.3 nm. For the ZnCoS sample (Fig. 2b) the analysis results indicate the presence of only sulfur impurity, and the average crystallite size of the ZnCoS solid solution was found as 22 nm.

Additional information on molecular residues in the samples after the synthesis is given by IR spectra (Fig. 3a). Broad absorption bands in the left part of the spectra with the maximum at ~3400 cm^{-1} correspond to hydroxyl groups; they partially disguise the informative bands of hydrocarbon stretching vibrations in the range 3000-2800 cm^{-1}. However, in the region of molecular fingerprints below 2000 cm^{-1} the spectral picture is sufficiently clear for the analysis. The IR spectral profile of the ZnMnS sample (gray in Fig. 3a) noticeably resembles the spectrum of thioglycolic acid chemisorbed on QD [28]. We mean the characteristic shape of the absorption curve in the range 3000-2000 cm^{-1} and dominant bands at 1580 cm^{-1} and 1406 cm^{-1}, corresponding to asymmetric and symmetric vibrations of carboxylates. At lower frequencies the similarity is violated, and therefore, the same bands with regard to peaks at 1305 cm^{-1}, 870 cm^{-1}, 650 cm^{-1}, and 483 cm^{-1} can indicate the occurrence of acetate ions, most probably, a zinc salt. The band at 1135 cm^{-1} is typical of sulfate ions (e.g., Na_2SO_4). The bands at 1620 cm^{-1}, 1110 cm^{-1}, and 630 cm^{-1} [29], which are observed in the spectrum, however, partially hidden by the neighboring absorption bands, are assigned to sulfides. The IR spectrum of ZnCoS does not give obvious evidence of the occurrence of either thioglycolic acid or acetates, however, the occurrence of sulfates (e.g., $ZnSO_4$) along with metal sulfides is more pronounced.

The experimental characterization of obtained QDs is completed by the examination of their optical properties. The absorption spectra measured in the reflection geometry (Fig. 3b) demonstrate the profile of an increase in the absorption with
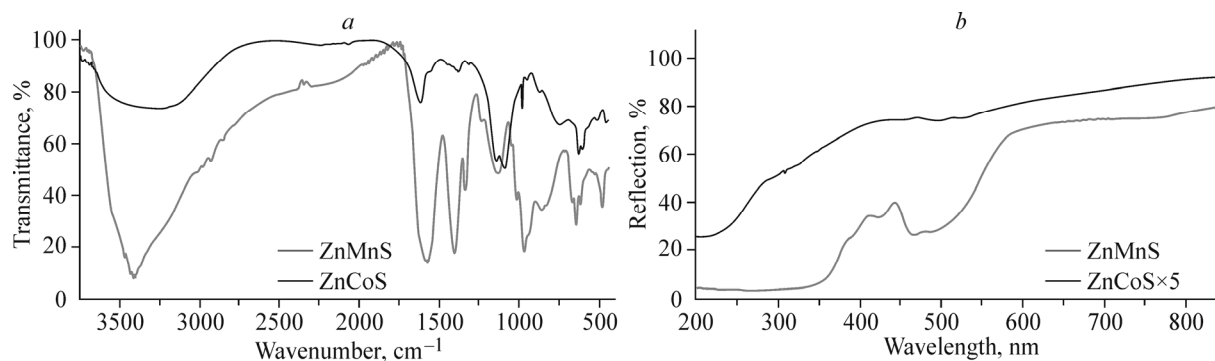

Fig. 3. IR (a) and optical (b) spectra of ZnMnS (gray) and ZnCoS (black) samples.

a decrease in the wavelength, which is common for semiconductor materials. The fundamental absorption boundary is located near 340 nm, which is characteristic of ZnS. At 470 nm there is pronounced absorption peak usually observed for MnS compounds.

Reviewing the experimental data, one may note that the TEM and DLS data are consistent with the estimate of the average crystallite size from the powder X-ray diffraction analysis. The double difference in the crystallite sizes of the samples indicates a difference in the particle formation process in the same temperature-time mode. Zinc and sulfur loss because of the concurrent processes during the synthesis, which were revealed by XRF, is aggravated by the formation of elementary sulfur as well as oxides of unreacted precursors, which were revealed by IR spectroscopy and taken into account in the analysis of diffraction patterns. Optical spectroscopy does not exclude the presence of some amount of monometal sulfide particles. In both dry state and solution the particles are characterized by some degree of aggregation, which can be decreased by a selection of the solvent and long-term ultrasound dispersion of the solution.

Based on DFT the structures of ZnS:Mn and ZnS:Co particles with a radius of 7 Å, which contain 68 atoms, were optimized. A consideration of particles with a radius of 7 Å is the first step in the investigation of the structures of real systems. The XANES spectra near the K-edge of doping metal were calculated for ZnS:Mn (Fig. 4a) and ZnS:Co (Fig. 4b) particles. The spectra were calculated for clusters representing fragments of crystalline ZnS [17], in which the central Zn atom is replaced by Mn or Co atoms (solid lines), for the optimized ZnS cluster with the subsequent substitution of the central Mn or Co atom (dashed lines), for the optimized structures of ZnS:Mn, ZnS:Co particles with the pre-optimization of the ZnS structure (dot-and-dash lines). It is seen that XANES spectra are sensitive to small changes in the local environment of doping atoms. This indicates the possibility to apply XANES spectroscopy to verify the structural parameters of transition metal solid solutions with ZnS. The question about the formation of solid solutions in the synthesized ZnMnS and ZnCoS systems under study can be further solved by the analysis of experimental XANES spectra.

In order to investigate the electronic structure of ZnS QDs doped with transition metal atoms, the total and partial DOS near the top of the valence band and the bottom of the conduction band of ZnS:Mn and ZnS:Co clusters were calculated. Obtained DOS for the optimized ZnS:Co particle are presented in Fig. 5. For comparison, Fig. 5 also presents total DOS of the wurtzite phase of crystalline ZnS. It is seen that because of Co-doping impurity new states arise in the band gap of ZnS, which are caused by the hybridization of Co d states and S p states.
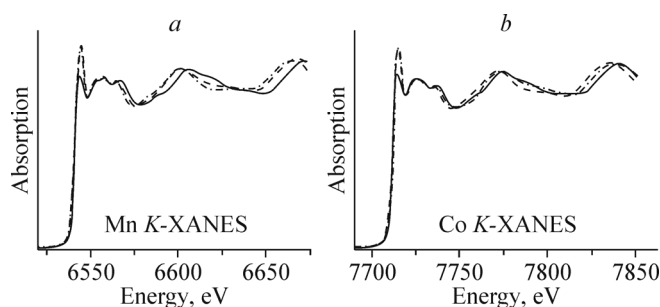

Fig. 4. Theoretical Mn K-XANES spectra of the ZnS:Mn particle (*a*) and Co K-XANES spectra of ZnS:Co (*b*). Solid lines show the XANES spectra calculated for particles representing fragments of crystalline ZnS in which the central Zn atoms are replaced by Mn or Co atoms. Dashed lines correspond to the spectra calculated for the optimized ZnS particle with the subsequent substitution for the central Mn or Co atom. Dash-and-dot lines show the spectra of the optimized structures of ZnS:Mn and ZnS:Co particles with the pre-optimization of the ZnS structure.
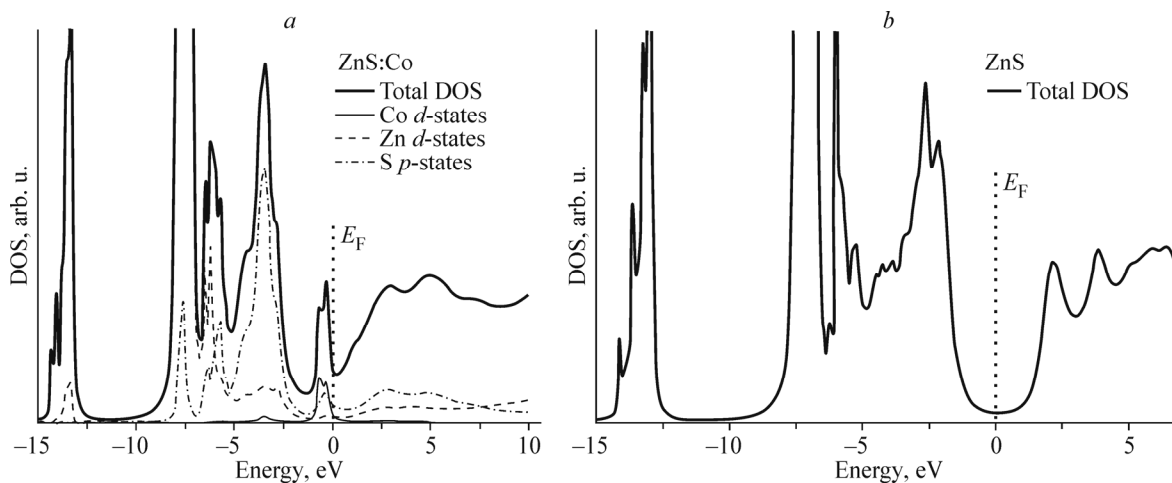
Fig. 5. Total DOS near the top of the valence band and the bottom of the conduction band of crystalline ZnS (*a*). Total and partial DOS of the ZnS:Co particle (*b*). The Fermi level position E_F is shown by vertical dotted lines.

CONCLUSIONS

This work presents QDs based on zinc sulfide, which represent a solid solution with doping manganese and cobalt atoms. X-ray diffraction data and the spectral analysis indicate the occurrence of impurity phases in the samples. The average particle size with manganese is 8 nm; it is almost twice as small as that with cobalt. The samples turned out to be differently stabilized by thioglycolic acid. All these factors give evidence of different dynamics of the particle formation under equal synthesis conditions, which requires further studies. The possibility of using XANES spectroscopy to verify the atomic structural parameters around the positions of doping transition metal atoms in QDs based on ZnS particles is shown.

REFERENCES

1. J. M. Costa-Fernandez, R. Pereiro, and A. Sanz-Medel, *TrAC Trends Anal. Chem.*, **25**, 207 (2006).
2. K. Park, J. Joo, S. G. Kwon, et al., *Angew. Chem. Int. Ed.*, **46**, 4630 (2007).
3. L. Bányai and S. W. Koch, *Semicond. Quantum Dots*, World Scientific, Singapore (1993).
4. X. Fang, T. Zhai, and U. K. Gautam, *Prog. Mater. Sci.*, **56**, 175 (2011).
5. R. N. Bhargava, D. Gallagher, X. Hong, and A. Nurmikko, *Phys. Rev. Lett.*, **72**, 416 (1994).
6. V. F. Agekyan and N. G. Filosofov, *Diluted Magnetic Semiconductors: Magnetic and Optical Properties* [in Russian], Manual, St. Petersburg Univ., St. Petersburg (2014).
7. G. Bunker, *Introduction to XAFS. A Practical Guide to X-ray Absorption Fine Structure Spectroscopy*, Cambridge: University Press, UK (2010).
8. A. N. Kravtsova, M. A. Soldatov, S. A. Suchkova, et al., *J. Struct. Chem.*, **56**, No. 3, 517 (2015).
9. A. N. Kravtsova, K. A. Lomachenko, S. A. Suchkova, et al., *Izv. RAN. Ser. Fiz.*, **79**, No. 11, 1612 (2015).
10. A. N. Kravtsova, S. A. Suchkova, M. B. Fain, and A. V. Soldatov, *J. Struct. Chem.*, **57**, No. 3, 491 (2016).
11. D. E. Dunstan, A. Hagfeldt, M. Almgren, et al., *J. Phys. Chem.*, **94**, 6797 (1990).
12. K. Sooklal, B. S. Cullum, S. M. Angel, et al., *J. Phys. Chem.*, **100**, 4551 (1996).
13. N. Karar, H. Chander, and S. M. Shivaprasad, *Appl. Phys. Lett.*, **85**, 5058 (2004).
14. C. Carrillo-Carrion, S. Cardenas, B. M. Simonet, and M. Valcarcel, *Chem. Commun.*, 5214 (2009).

15. L. Cao, J. Zhang, S. Ren, and S. Huang, *Appl. Phys. Lett.*, **80**, 4300 (2002).

16. Q. Xiao and C. Xiao, *Opt. Mater.*, **31**, 455 (2008).

17. E. H. Kisi and M. M. Elcombe, *Acta Crystallogr. C*, **45**, 1867 (1989).

18. G. Kresse and J. Furthmüller, *Comput. Mater. Sci.*, **6**, 15 (1996).

19. J. P. Perdew, K. Burke, and M. Ernzerhof, *Phys. Rev. Lett.*, **77**, 3865 (1996).

20. G. Kresse and D. Joubert, *Phys. Rev. B*, **59**, 1758 (1999).

21. H. Modrow, S. Bucher, J. J. Rehr, and A. L. Ankudinov, *Phys. Rev. B*, **67**, 035123 (2003).

22. Y. Joly, *Phys. Rev. B*, **63**, 125120 (2001).

23. S. A. Guda, A. A. Guda, M. A. Soldatov, et al., *J. Chem. Theory Comput.*, **11**, 4512 (2015).

24. A. L. Ankudinov, C. E. Bouldin, J. J. Rehr, et al., *Phys. Rev. B*, **65**, 104107 (2002).

25. Yu.Yu. Lurie, *Handbook of Analytical Chemistry* [in Russian], 5th ed., Khimiya, Moscow (1979).

26. *Card No 401289, PDF-2, The International Centre for Diffraction Data*; http://www.icdd.com.

27. *Card No 750605, PDF-2, The International Centre for Diffraction Data*; http://www.icdd.com.

28. L. Alamo-Nole, S. Bailon-Ruiz, O. Perales-Perez, et al., *Anal. Methods*, **4**, 3127 (2012).

29. G. Murugadoss, *J. Lumin.*, **131**, 2216 (2011).